# Development of biomass-based slurry for the manufacture of furan/cellulose composite by cast molding and 3D printing

Khaoula Bouzidi, Didier Chaussy, Alessandro Gandini, Roberta Bongiovanni, Davide Beneventi

# DEVELOPMENT OF BIOMASS-BASED SLURRY FOR THE MANUFACTURE OF FURAN/CELLULOSE COMPOSITE BY CAST MOLDING AND 3D PRINTING

Khaoula Bouzidi,[1,*] Didier Chaussy,[1] Alessandro Gandini[1], Roberta Bongiovanni,[2] Davide Beneventi[1]

[1] Univ. Grenoble Alpes, CNRS, Grenoble INP (Institute of engineering Univ. Grenoble Alpes), LGP2, 38000 Grenoble, France

[2] Department of Applied Science and Technology, Politecnico di Torino, Torino, 10129 Italy

* Corresponding author.

**ABSTRACT:** The present study aims to develop a green composite based on two biomass-based components via the curing of an oligomeric furfuryl resin (OFR) coupled with 18-31 wt% cellulose powder. The curing was performed in an atmospheric pressure open air oven. The chemical composition of the used pre-polymer was characterized with FT-IR and NMR spectroscopy and its curing reaction was followed by DSC. The final cured composites were characterized to investigate the effect of cellulose addition on their morphology, dimensional stability and thermo-mechanical performances. The manufactured composite showed good thermal stability up to 200°C with a storage modulus higher than 2 GPa, and a mass loss under 3%. Moreover, the filler improved the composite dimensional stability upon crosslinking by 38% and the mechanical performances with respectively 15% and 40% increase in the Young's and flexural moduli. By the same token, cellulose prevented the typical foaming of PFA resins crosslinked at high temperature and low pressure. Preliminary tests highlighted the excellent processability of the developed composite which was used to manufacture a static demonstrator coupling different fabrication techniques, i.e. 3D printing (direct ink writing), high temperature compression molding and CNC machining.

**KEYWORDS:** Bio-based; Furan; Cellulose; Composites; Thermomechanical properties

**ABSTRACT GRAPHICAL**

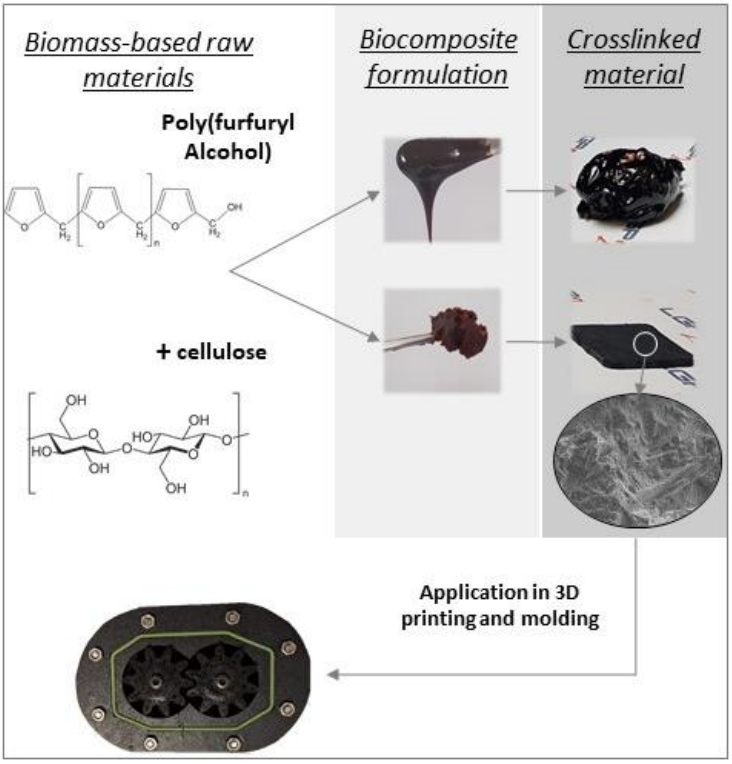


## 1 INTRODUCTION

In recent years, sustainability has gained a large interest in the manufacturing of products due to the dwindling of fossil resources and the growth of environmental awareness. Because of these economic and ecological reasons, the use of natural fibers has become more attractive in composite production owing to their availability and sustainability. However, the most polluting element is the fossil-based polymer matrix, and therefore the use of renewable polymers was suggested for the production of totally bio-based composites. One such bio-based and the readily available polymer is poly(furfuryl alcohol) (PFA) which is produced via the acid-catalyzed polymerization of furfuryl alcohol (FA). FA is industrially produced via the hydrogenation of furfural, which is obtained from a variety of pentosane-rich biomass residues, such as sugar cane bagasse, corn cobs, oat lulls, and rice husks [1, 2].

The polycondensation of FA proceeds following two alternative steps, namely head-to-tail [1] or head-to-head [2] and the latter reaction produces an unstable ether moiety which loses formaldehyde in an acidic medium, thereby giving the same methylene bridge formed in reaction [1], as shown in Figure 1 [3].

This simple growth giving 2,5-furanmethylene units is however perturbed by two reactions involving the polymer, namely the formation of conjugated sequences by loss of hydride ions and protons, leading to a progressive bathochromic shift in color all the way to a black product, accompanied by a polymer-to-polymer Diels-Alder coupling resulting in a crosslinked material [3].

This complex structure has puzzled chemists for decades. As analysis techniques evolve, scientists had more data and hence more information about the structure emerged putting together various secondary reactions [4].

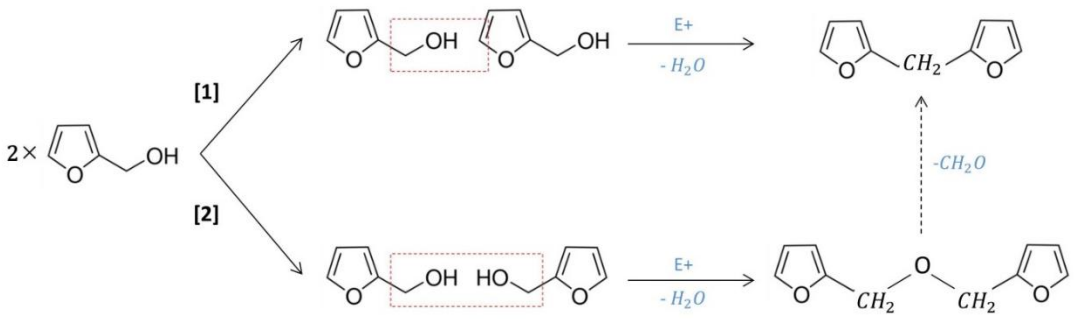


**Figure 1:** Stepwise polycondensation reaction of FA according to the two different pathways

The ensuing FA-based resins (PFA) have found numerous applications, thanks to their excellent flame and chemical resistance and low smoke emission, including metal-casting cores, wood adhesives and binders, coatings, and a precursor to carbonaceous products [3].

Recently, they have also been used in the production of composites along with synthetic and natural fibers, e.g. by mold compression of flax and kenaf prepregs [5, 6] and woven glass prepregs [7]. The challenge of the use of this resin was mainly foaming and water condensation which causes high porosity in the composites. The porosity is mainly affected by the moisture content in the composite which should be limited [8] and the condensation of vapor produced during polymerization. The condensation water should be evacuated during the curing process to minimize its effect on porosity [7], which leads to complicated processing of the composite.

PFA has also been coupled with lignocellulosic particles such as humins [9], cork residues [10], lignin [2], and sisal whiskers [11], which displayed good compatibility and improvement in the mechanical performances of the

composites. More recently, low concentrations of PFA were added to natural fibers such as micro-fibrillated cellulose [12] for mechanical reinforcement, and bamboo [13] for the improvement of physical-mechanical properties and decay resistance.

An overview of the state of the art of composites developed with PFA highlighting their mechanical and thermal properties is presented in Table 1. According to this data, one can notice that PFA has been mainly coupled either with different classes of natural non-wood fibers such as flax, sisal, and bamboo. These composites were manufactured using different methods but compression is always applied and, if not, PFA was used to produce thin films pobably due to the high porosity which this resin can generate when manufacturing bulk structures. In terms of mechanical properties, it was reported that the neat PFA has a stiffness below 1 GPa (tensile mode) and tensile strength of about 10 MPa [5, 14]. After the addition of a continuous reinforcing phase, for instance, aligned flax fiber woven textile, the stiffness of the resulting composite reached a value of 25 GPa and its strength attained 211 MPa. However, when adding discontinuous filler we notice a limited improvement in Young's modulus which remains under 2 GPa and a considerable improvement in the strength of about 400% compared to the neat polymer. In terms of thermal properties, the results can be quite dispersed depending on the used polymer and filler with a $T_g$ ranging from 80°C to over 130°C and a storage modulus over 1 GPa at 160°C in some cases. The addition of some of these fillers (especially nanoparticles) served to confer the polymer with new properties such as electrical conductivity, long wear life, and superhydrophobic surface.

**Table 1:** A summary of research work on PFA-based composites and their mechanical and thermal properties.

| **Fillers** | **Filler's concentration** | **Manufacturing methode** | **Curing conditions** | **Mechanical properties** | **Thermal properties** | **Ref** |
|---|---|---|---|---|---|---|
| **Flax** fibers mat | **50 wt%** | **Compression** molding 2.2 MPa | 150°C | Young's modulus= 12.2 GPa Rupture strength= 95 MPa | Storage modulus= 1 GPa at 160°C Tg= 105°C | [15] |
| **flax** fibers mat | **60 wt%** | **Vacuum bag** | 150°C for 15 min | Young's modulus= 8.5 GPa Tensile strength= 64 MPa | N.A | [16] |
| **Flax** fibers non-woven | **57 wt%** | **Compression** molding 2 MPa | 150°C | Young's modulus= 9 GPa Rupture strength= 48 MPa | N.A | [6] |

| Fillers | Filler's concentration | Manufacturing methode | Curing conditions | Mechanical properties | Thermal properties | Ref |
|---|---|---|---|---|---|---|
| **Cellulose whiskers** | **0.75 wt%** | **Open-air casting** | 130°C for 75 min + 210°C for 105 min | Young's modulus= 1 GPa Rupture strength= 32 MPa | Char residue at 800°C 50 wt% | [17] |
| **Flax** fiber fabric | **N.A** | **Compression** molding | 140°C | Young's modulus= 25 GPa Tensile strength= 211 MPa | N.A | [18] |
| **Sisal whisker** | **2 wt%** | **Open-air** molding | 70°C, 100°C and 150°C | Storage modulus= 2.1 GPa at 25°C | Char residue at 800°C 50 wt% Tg= 70°C | [11] |
| **Kenaf fibers** | **20 wt%** | **Compression** molding 7 MPa | 60°C for 4 h + 80°C for 4 h + 110°C for 1 h | Young's modulus= 1.25 GPa Tensile strength= 42 MPa | Storage modulus= 0.5 GPa at 150°C Tg= 95°C Char residue at 800°C 45 wt% | [5] |
| High tenacity **rayon** filaments | 64 wt% | **Compression** molding 10 MPa | 40°C for 12 h + 60°C for 12 h + 80°C for 6 h | Young's modulus= 5.5 GPa Tensile strength= 120 MPa | Tg=122°C Storage modulus= 1.5 GPa at 160°C 35 wt% Char residue at 600°C | [19] |
| **MFC-L gel** | 50 wt% | **Open-air** casting | Freeze-drying | Compression modulus= 1 MPa Compression strength= 0.21 MPa | 20 wt% char residue at 800°C | [12] |
| **Cork powder** | **25 wt%** | **Compression** molding 1 MPa | 160°C | Young's modulus= 180 MPa Tensile strength= 6.5 MPa | Storage modulus= 0.8 GPa at 160°C | [10] |
| **Bamboo** fibers | 30 wt% | Pressure **impregnation** | 120°C for 5 h | Modulus of elastic= 6 GPa Modulus of rupture= 15 GPa | 20 wt% char residue at 800°C | [13] |

In this study, a totally biomass-based composite was developed coupling a commercial oligomeric furfuryl resin (OFR) with cellulose powder by simple casting and curing under atmospheric pressure. The cellulose powder allowed to improve the intrinsic low viscosity of the OFR and favored vapor degassing during thermal curing thus leading to the formulation of a highly viscous composite paste that can be effectively processed both by 3D printing and thermo compression molding. 3D printed and molded/milled objects displayed excellent shape fidelity and

porosity/mechanical properties in line with those obtained for casted samples thus paving the way for the use of cellulose/OFR composites in advanced manufacturing processes other than prepreg or sheet compression molding.

# 2 MATERIALS AND METHODS

## 2.1 Materials

A commercial OFR and a latent catalyst were kindly supplied by Transfurans Chemicals (Belgium). The commercial resin contains 7.5 wt% water and less than 1% of free FA monomer. According to the supplier's information, the polymer can be stored for a long time at temperatures between 20 °C and 25 °C, and the shelf life of this kind of resin can reach 18 months under ambient conditions [20].

Commercial cellulose fibers were kindly supplied by the Rossow Industry. The fibers have a powdery aspect and, according to preliminary SEM analysis, shown in Figure 2, the fibers are stocky particles with an approximated aspect ratio of 5. The water content of the cellulose was measured to be 4.58 ±0.05 wt%. As determined using the image granulometric analysis given in Figure 2, 50% of the cellulosic particle have a size smaller than 9.8 µm.

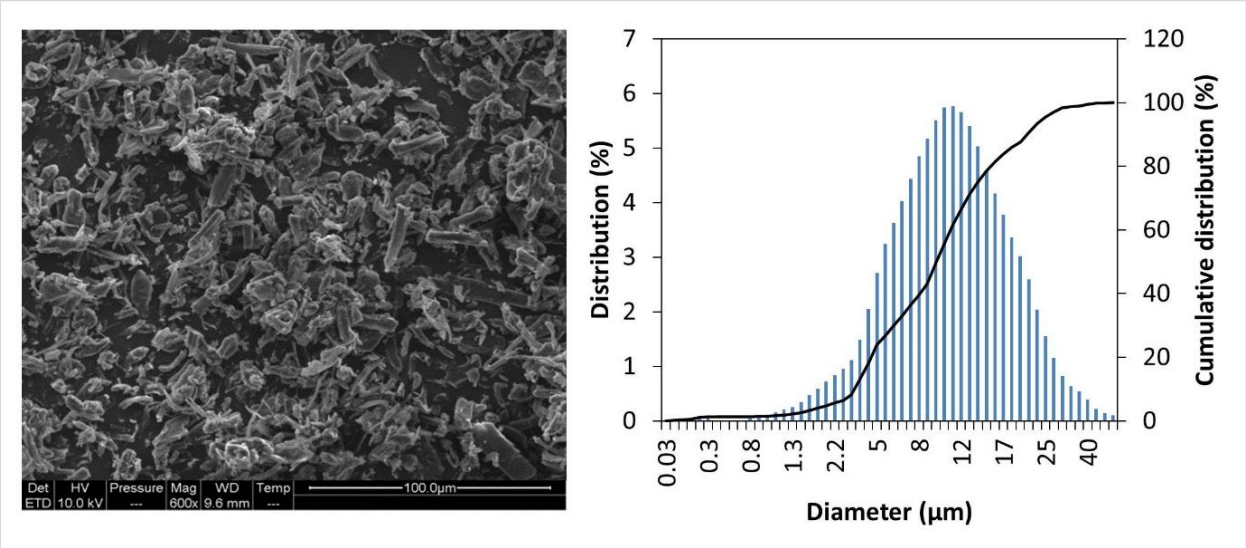


**Figure 2:** SEM photograph of the dry cellulose powder and its particles size distribution measured using a granulometer (Cilas particle size analyzer 1190) based on the Fraunhofer method.

## 2.2 Composite fabrication

The composite slurry was prepared by first adding the catalyst to the resin and manually mixing the two fluids. The mixture was then put in a planetary mixer and the cellulose powder was gradually added and the whole was blended

for at 30 min. The paste was then placed in a refrigerator at 4-5 °C before further processing. In this study, different formulations were tested with different cellulose fractions, as shown in Table 2.

The weight fractions of the cured composite were calculated considering that during the crosslinking 100% of the water was evaporated (added water and condensation water). The density of the cured OFR is estimated to be 1.36 $g.cm^{-3}$ [7].

**Table 2:** Different tested composite formulation's compositions.

| | Slurry component by weight (wt%) | | | Slurry component by volume (vol%) | | | Composite by weight (wt%) | |
|---|---|---|---|---|---|---|---|---|
| **Formulation** | **PFA** | **Solvent** | **Cellulose** | **PFA** | **Solvent** | **Cellulose** | **PFA (Wm)** | **Cellulose (Wf)** |
| **Neat PFA** | 91.19 | 8.81 | 0 | 97.73 | 2.27 | 0 | 100 | 0 |
| **PFA-Cell16-B** | 76.60 | 7.40 | 16.00 | 81.84 | 4.95 | 13.20 | 82.22 | 17.78 |
| **PFA- Cell19-B** | 73.65 | 7.12 | 19.23 | 79.23 | 4.79 | 15.98 | 78.72 | 21.28 |
| **PFA- Cell22-B** | 70.93 | 6.85 | 22.22 | 76.78 | 4.64 | 18.58 | 75.51 | 24.49 |
| **PFA- Cell25-B** | 68.39 | 6.61 | 25.00 | 74.47 | 4.51 | 21.03 | 72.55 | 27.45 |
| **PFA- Cell28-B** | 66.03 | 6.38 | 27.59 | 72.30 | 4.37 | 23.33 | 69.81 | 30.19 |
| **PFA- Cell29-B** | 65.14 | 6.29 | 28.57 | 71.46 | 4.32 | 24.21 | 68.77 | 31.23 |

The cold slurries were placed in an oven at 50°C for 5 min to decrease their viscosity and facilitate their processing. The bio-composites were prepared using a simple hand casting in open poly(tetrafluoroethylene) molds. The casting was done manually and without any additional constraints, yet avoiding creating voids because of the sticky nature of the slurries. The molds were then placed in the oven at 90°C for an open-air crosslinking overnight. A post-curing was then performed for 3 hours at 130°C. The processability of the developed paste was tested using a direct ink writing (DIW) 3D printer and by CNC milling composite plated manufactured by hot compression molding (2-4 MPa and 100°C).

## 2.3 Analyses and characterization techniques

To analyze the structure and composition of the commercial OFR, 13C and 1H NMR investigations were done on both liquid and solid polymers. Spectroscopic measurements were recorded on a Bruker AVANCE400 spectrometer (Billerica, MA, USA) equipped with a 5 mm BB/19F-1H/d Z-GRD probe operating at 100.612 MHz for 13C, and 400.130 MHz for 1H. For solid-state RMN the sample was compacted in 4 mm ZrO2 rotors while the liquid NMR

measurements were performed on OFR samples dissolved in DMSO-d6 and placed in a 10-mm tube. For further investigation, Fourier Transform Infrared (FT-IR) spectroscopy analyses were also conducted using a PerkinElmer FT-IR spectrometer (Perkin Elmer, USA). For solid samples analysis, each sample was grounded and then mixed with KBr powder with a ratio of 1:125 for pellets preparation. The spectra were acquired in a frequency range of 4000- 500 $cm^{-1}$ with a resolution of 4 $cm^{-1}$ and then corrected with the environmental spectrum. For liquid resin analysis, the sample was placed between two NaCl plates after removing the water.

The thermal analysis of the thermosetting resin was performed by Differential Scanning Calorimetry (DSC) (TA DSC Q100). An average of 10 mg of each sample was placed in a closed aluminum crucible and heated from 40°C to 200°C at 5°C.$min^{-1}$ under airflow. The thermogravimetric analysis (TGA) of the composites was performed on TGA-DSC3+ Mettler Toledo. The samples were heated from room temperature to 1000°C with a temperature ramp rate of 10°C.$min^{-1}$. The thermo-oxidative degradation of the composites and the neat PFA network were studied under a 40 mL.$min^{-1}$ oxygen flow, and further tests were performed under a nitrogen flow of 40 mL.$min^{-1}$.

To evaluate the shrinkage upon crosslinking of the neat PFA and the bio-composites, the French standard NF 51-401 was followed. 5 specimens of 80 mm × 10 mm × 4 mm were prepared for each sample according to the protocol previously described. The samples were then placed in a normalized atmosphere for 24 hours before measuring their length L' with 0.05 mm precision after curing, using a caliper. For every specimen, the measure was repeated at least 5 times. The shrinkage upon curing R% was calculated according to equation (1):

$$R\ (\%) = L'/L \times 100 \qquad (1)$$

To measure open and close porosity in the composite with different cellulose content, 2.5 cm square specimens with 2 mm thickness were cured. The Buoyancy method was used (ASTM D792) to measure the experimental density ($D_{ex}$) with a surfactant aqueous solution as a test liquid. The theoretical density ($D_{th}$) was calculated by considering that the cured PFA was perfectly compact using the rule of mixtures. The porosity percentage in the composites was calculated based on the equation (2):

$$P\ (\%) = ((D_{th} - D_{ex}) \times 100)/D_{th} \qquad (2)$$

To assess the composite sensitivity to humidity, samples of the cured composite and neat cellulose along with cellulose powder were placed in a Varimass apparatus (TechPap). The relative humidity (RH) was controlled and the mass variation was recorded during the entire test via an integrated precision balance. The humidity program

consisted of 3 cycles. In the first cycle, the humidity was fixed at 50% for 2 hours. The second cycle started with two hours at low humidity (20%) followed by two hours at 50%. The third cycle started with two hours at a high humidity level (90%) followed by stabilization at 50% for two extra hours.

The morphology of both fillers and the composite were investigated by scanning electron microscopy (SEM). The specimens were gold coated and examined using a QuantaFEG250 instrument. The accelerating voltage was fixed at 2.50 kV and the magnitude between 60 and 2000.

The dynamic mechanical properties, such as the storage modulus E', were studied with a Dynamic Mechanical Analyzer (DMA). Tests were realized using the 3-points bending mode with a temperature scan ranging from 25 °C to 300 °C at 2 °C.min$^{-1}$ at a frequency of 1 Hz. The static force had an average of 25 N and the dynamic deformation was ±15 μm. The samples' dimensions were 40×10×4 mm (length, width, and thickness) and were measured precisely for every specimen before the scan. At least 3 specimens per sample were analyzed.

Before any mechanical test, the composites were conditioned at 23 °C and at 50% relative humidity for at least 16 h. The mechanical properties were tested with an Instron Universal Testing Machine and the data analyzed with the help of the Blue Hill software. The tensile test was performed according to the ISO 527 standard using the 5A specimen dimension and a crosshead speed of 2 mm.min$^{-1}$. The flexural properties were measured according to ISO 178 at a crosshead speed of 2 mm.min$^{-1}$. The obtained data were the average of 10 to 15 measurements. The specimens were prepared by open-air casting molding, as described above and therefore shrinkage of up to 5% of the dimensions took place. The surfaces of the samples were polished by sandblasting and the exact dimensions were measured before every test.

# 3 RESULTS AND DISCUSSION

## 3.1 Resin investigations

The $^{1}$H NMR spectrum of the commercial OFR in Figure 3 shows a clear peak around 6.2 ppm, which reflects the resonance of the H3 and H4 protons of the furan ring. The peak of the H5 proton around 7.5 ppm is surprisingly very weak because, in the case of the oligomerization of exclusively FA monomers, those protons will be present at least at one of the extremities of the formed oligomers [3].

On the other hand, if one compares the signal of the -$CH_2$- methylene bridge protons between two furan rings around 3.8 ppm and the signal of $CH_2$-O protons, which can be either those derived from the terminal $CH_2OH$

groups or those in the ether bridge formed after the condensation according to reaction (2), one can notice that the latter is uncommonly more important [3, 21, 22]. Around 5.3 ppm is the signal of the $CH_2OH$ hydroxyl protons which is a much more important peak than that of the free H5 protons. The strong peak at 3.3 ppm is related to the water protons, assigned to the remaining moisture in the commercial product.

On the $^{13}C$ NMR spectrum of the commercial OFR, shown in Figure 4, the signals between 156 ppm and 149 ppm match the C3 and C4 carbons, and those of the C2 and C5 are found between 110 and 113 ppm, which reveals the presence of furan rings. Comparing the methylene bridge and the ether bridge signals, at respectively 27 ppm and 56 ppm, one can see again a stronger presence of the latter. Around 175 ppm, one can also detect a modest signal of carbonyl groups which is due to the furan ring-opening due to its minor acid hydrolysis during the oligomerization [23].

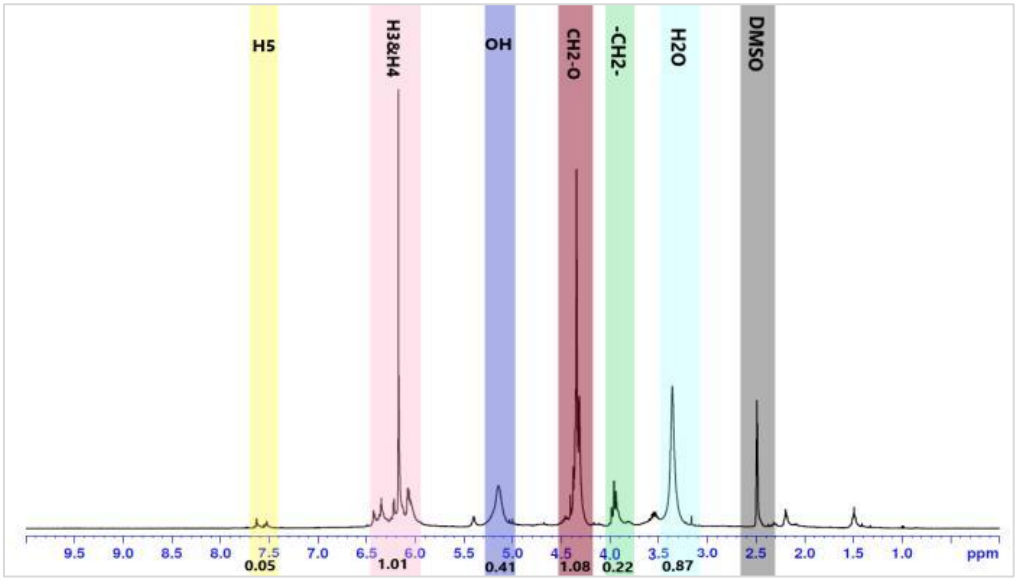


**Figure 3:** $^{1}H$ NMR spectrum of the commercial OFR in DMSO-$d_6$

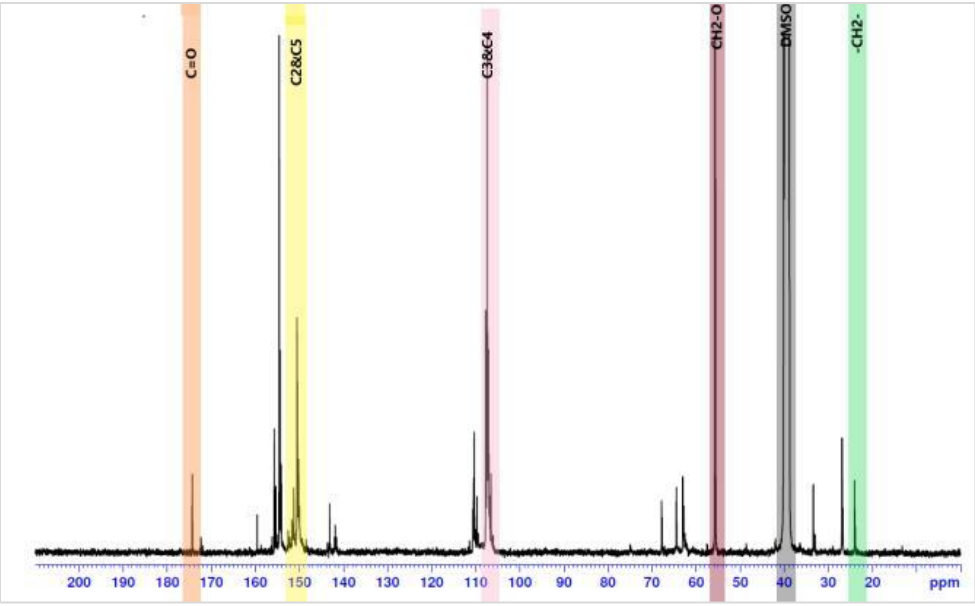


**Figure 4:** $^{13}C$ NMR spectrum of the commercial OFR in DMSO-$d_6$

Examining the FT-IR spectra on Figure 5, the first observation relates to the important signal around 3400 $cm^{-1}$ of the OH groups of the "dry" product which we have verified on the $^{1}H$ NMR spectrum, probably partially arising from the residual moisture in the resin. But these hydroxyls are mainly due to the terminal groups of the oligomers, which are the reason behind the partial solubility in water of the commercial resin thanks to the polarity of its molecules. The presence of the furan ring is proven by the two signals around 1000 and 800 $cm^{-1}$. One can also distinguish the typical double peak around 2900 $cm^{-1}$ of the $CH_2$ groups. The peak around 1200 $cm^{-1}$ is indicative of ether bonds ($CH_2$-O-$CH_2$). Around 1720 $cm^{-1}$ a peak of the carbonyl groups is due to the furan ring opening during the oligomerization, as discussed above [3, 21].

According to the NMR data of the commercial oligomer, the ether bridges are more frequent than the methylene ones, and terminal $CH_2OH$ groups are much more frequent than unsubstituted H5 end groups, both facts being entirely uncommon for typical FA oligomers, in view of the established mechanism shown in Figure 1. Indeed, in the case of the predominance of reaction (2) without loss of formaldehyde, and hence the important presence of ether bridges, the condensation would be soon blocked for lack of $CH_2OH$ moieties, i.e. one would only be faced with oligomers ending with 2 unreacted protons at the C5 positions, which is clearly not the present situation. Conversely, the strong presence of hydroxyl groups on the NMR and FTIR spectra versus a very limited sign of the proton at the C5 position, suggests that these oligomers are ending predominantly with hydroxymethyl groups rather

than a furan ring with an unreacted H5 proton. It seems logical to suggest therefore that the synthesis of the commercial OFR required the concomitant use of FA and another furan monomer capable of generating a high frequency of ether bridges and terminal $CH_2$-OH groups, e.g. 2,5-hydroxymethylfuran.

This structural investigation showed that the interest of the product developed by Transfurans in that it allows water compatibility while maintaining the potential to polymerize and crosslink following essentially the same mechanisms discussed above for FA alone, using a temperature activation catalyst which allows the process to occur upon heating the system, as detailed below.

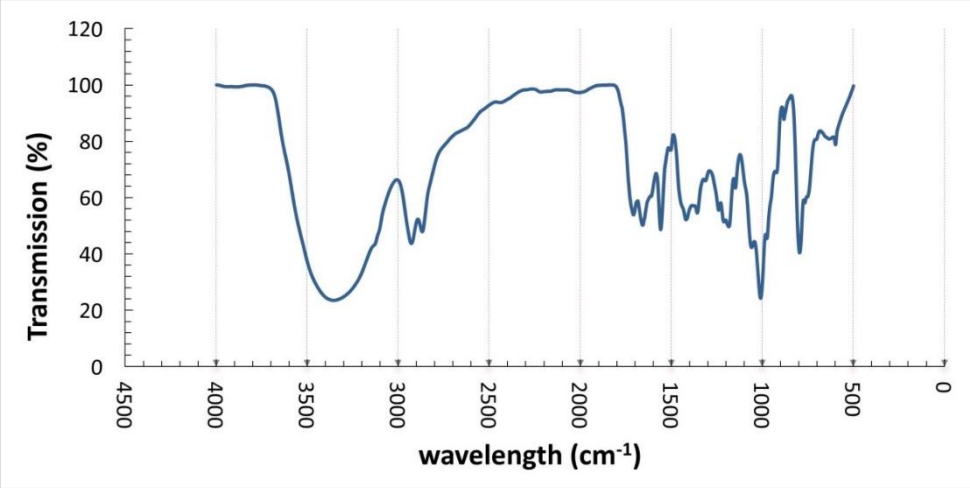


**Figure 5:** FT-IR spectrum of the commercial OFR

## 3.2 Crosslinking thermal analysis

Different PFA/catalyst ratios were analyzed by DSC at a 5°C.min$^{-1}$ heating rate. The PFA samples were prepared by diluting the commercial product with 15 wt% water and adding the catalyst at 0, 2, 5, and 15 wt%. On the DSC thermograms at different catalyst content, shown in Figure 6 and summarized in Table 3, the variation of the exothermic network-polymerization peak can be observed. The higher the catalyst concentration, the more pronounced the exothermic peak and the lower the exothermic peak temperature. In the same Figure, one can also see that the addition of the catalyst is essential for curing since, in the absence of catalyst, one cannot observe any exothermic peak, but only the endothermic peak of water evaporation at around 100°C. The increase in catalyst concentration up to 15 wt% induced a more exothermic (the maximum heat flow at the peak increases) and rapid reaction (lower onset temperature) which, in the case of PFA, can lead to the quick evaporation of residual water and foaming/high porosity. When adding 5 wt% of catalyst the curing heat has a similar value as when adding 15 wt%

catalyst (292-309 $J.g^{-1}$), thus suggesting that 5 wt% of catalyst is enough for a total crosslinking of the polymer in the tested conditions.

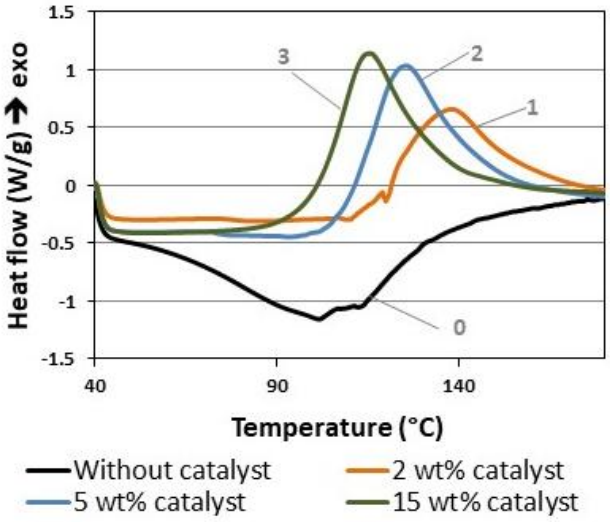


**Figure 6:** Curves of DSC scans of PFA containing different catalyst concentrations at a heating rate of 5°C.$min^{-1}$. The given numbers corresponding to different codes of samples detailed in Table 3.

On the other hand, the use of only 2 wt% of the catalyst seems to be insufficient for rapid curing because the reaction curing heat is around 262 $J.g^{-1}$, well below the enthalpy of 300 $J.g^{-1}$ measured when adding 5-15 wt% of catalyst. This reduction is supposed to be due to the fact that this low amount of catalyst is not capable of reaching all the reactive sites in the resin network leading to an incomplete crosslinking reaction [24, 25, 7].

It can be concluded that 5 wt% seems to be the best catalyst concentration to minimize the lower water content (the catalyst is water-based) while keeping a rapid curing rate with high conversion and a limited exothermic reaction peak.

**Table 3:** Summary of DSC scans data.

| Sample code | Catalyst content (wt%) | Onset Temperature (°C) | Peak temperature (°C) | Reaction enthalpy ($J.g^{-1}$) |
|---|---|---|---|---|
| 1 | 2 | 119 | 137 | 262 |
| 2 | 5 | 109 | 124 | 309 |
| 3 | 15 | 100 | 114 | 292 |

## 3.3 Water absorption under controlled relative humidity

The capacity of water absorption and desorption of the neat cured PFA, cellulose powder, and the composite was assessed with the Varimass device. Mass gain and loss during the different relative humidity levels are gathered in Figure 7. Cellulose contains hydroxyl groups that can interact with water molecules which makes this biopolymer highly sensitive to humidity. As one can notice in Figure 7, after mass stabilization at 50% of relative humidity, the cellulose lost up to 1.5% of its weight upon desorption at low humidity levels. At a high humidity level (90%), cellulose gained weight rapidly to reach 5% in two hours. On the other hand, cured PFA is a matrix insensitive to water. Therefore, it is expected that the number of OH groups in FA, available for hydrogen bonding with water molecules, was reduced during PFA polymerization, resulting in a non/slightly-polar polymer. As shown in Figure 7, the weight of the specimen was stable with virtually no mass variation. The composite with up to 27 wt% of cellulose remained insensitive to water its mass variation does not exceed 0.1%, even at high humidity levels. The composite nevertheless is slightly more sensitive to humidity compared with that of the neat matrix. These curves suggest that the ensuing composite is not sensitive to humidity despite the high cellulose fraction, a fact that can be explained by the encapsulation of cellulose particles in the hydrophobic polymer matrix. These findings are in agreement with a previous works [26],[27, 28]. Hence, the important cellulose content in the composites developed in the present work should not disrupt the outstanding performance of PFA polymers such as insensitivity to moisture and aging, thermal stability, and water resistance.

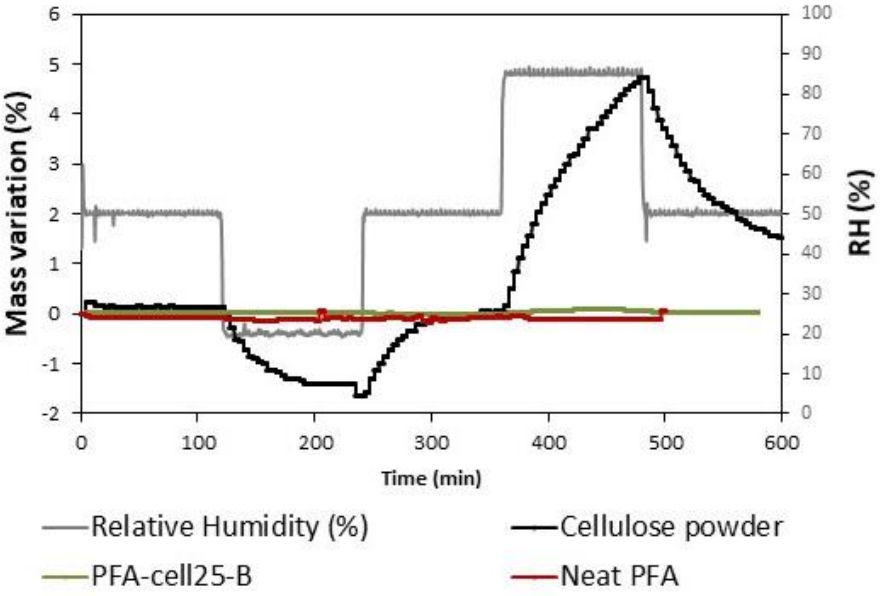


**Figure 7:** Water absorption of composites, neat PFA, and cellulose under controlled relative humidity.

## 3.4 Effect of cellulose on porosity and shrinkage

### 3.4.1 Effect of cellulose on foaming and porosity

One of PFA major issues is the high water content in the resin and the water generated by the condensation reactions during curing. This issue is particularly noticeable in composite manufacturing because it leads to high porosity and low dimensional stability. Other parameters can trigger pores formation in the furanic resin, but moisture content and viscosity are the dominant factors [8].

The used commercial PFA contains 7.5 wt% of water and generates over 2 wt% during curing [29], added to over 1.75 wt% of water brought by the catalyst. Therefore, at least 11 wt% of the resin's weight should be eliminated during the curing phase, which promotes porosity when the gas release is blocked. This important water content can lead to foaming caused by water boiling during the curing process especially for samples with thick walls which blocks the evacuation of gases through the structure. The foaming is particularly noticeable when the curing kinetic is fast, leading to a low gel time which interferes with gas elimination and hence the bubbles can be trapped inside the rubbery polymer matrix.

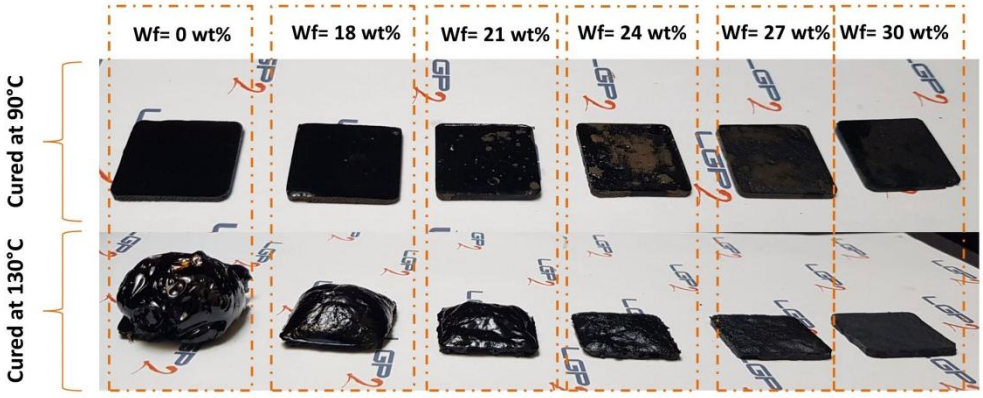


**Figure 8.** Photographs of different composites aspect cured overnight at 90°C and 130°C.

To further investigate the effect of cellulose on the porosity caused by the water evaporation during curing, the prepared formulations were cured in the oven, but at a higher temperature (around the exothermic peak of the curing reaction) to favor resin foaming and to assess the effect of cellulose on this phenomenon. Some samples fluffed up and the porosity could not be accurately measured. However, the effect of cellulose is clearly shown in Figure 8. One can notice that when curing at 90°C, below the water boiling temperature, the composite with or without cellulose did not foam, but still displayed micro and macro-porosity. When curing at 130°C, above the water boiling point, and with a lower gel time, the resin foamed because of the internal pressure due to gases and blocked by the external rubbery resin layer, as is illustrated in Figure 9-(a). This foaming was mitigated by the addition of cellulose, particularly in the PFA-Cell25-B composite. This effect can be related to the percolation of highly hydrophilic cellulose fibers which helped steam diffusion through the fibrous network without causing any noticeable deformation in the composite showed in Figure 8 and explained in Figure 9-(b).

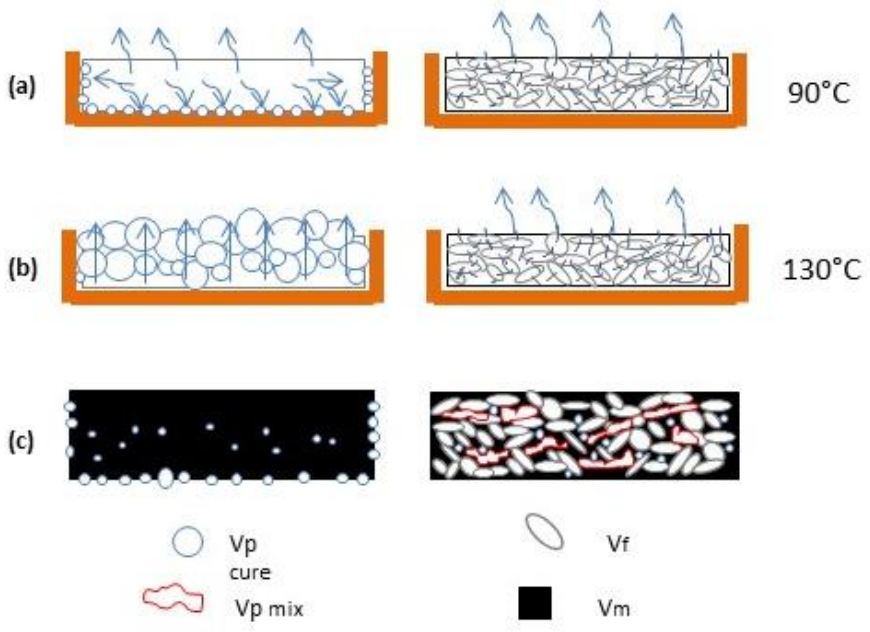


**Figure 9:** Illustration of the foaming and porosity formation phenomenon under different conditions. (a) Representation of the water evaporation and porosity formation in the mold at 90°C of the neat PFA resin (on the left) and the cellulose-based slurry (on the right). (b) Water evaporation at 130°C through neat PFA with foam formation under the evaporation forces and through cellulose-based slurry. (c) a representation of the different types of forms porosity in molded cured neat PFA and in the biocomposite. Vp cure presents the porosity volume caused by the degassing during the curing, Vp mix the porosity incorporated in the paste during the mixing, Vm is the volume occupied by the matrix, and Vf is that occupied by the fillers.

As shown in Figure 10, and in line with the above explanations, the neat cured PFA displayed almost no internal pores, but one can distinctly see macro-pores with perfect circular shapes all over the surface (Figure 10-(b)), showing the presence of air bubbles leaving the resin after water evaporation. These pores were more visible on the surface in contact with the mold, which obstructed bubbles degassing, as illustrated in Figure 9-(a). On the other hand, for the PFA-Cell25-B composite, one can notice on Figure 9-(c) numerous internal pores with different sizes and shapes, but mostly oval and recumbent along the casting direction. The surface of the specimen is smooth and presents no bubble marks.

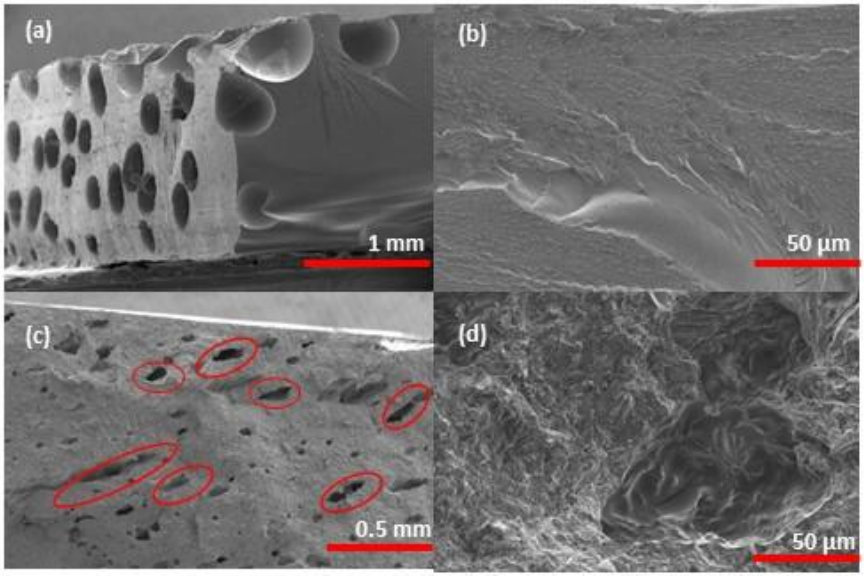


**Figure 10:** SEM images of several cured (90°C) PFA surface: (a) surface of the cured specimen of neat PFA, (b) fractured surface of neat PFA, (c) PFA-Cell25-B composite fractured surface, (d) zoom on the pores in PFA-Cell25-B composite.

This porosity might be mainly due to manual molding and mixing and not to vapor bubbles which were probably, as discussed above, drained through the fibrous network. On the micrograph in Figure 10-(d) one can visualize the fibers network. However, pores formation by vapor generation can still be possible and we suppose that they partially coalesced with the pre-existing air bubbles in the composite.

### 3.4.2 Study of the porosity origin

The porosity content (Vp %) of different composites is displayed in Figure 11. The pure PFA resin cured at 90°C had 8.8% porosity which is in agreement with the porosity found in a previous work for the same commercial PFA resin using the double-vacuum-bag technique [29].

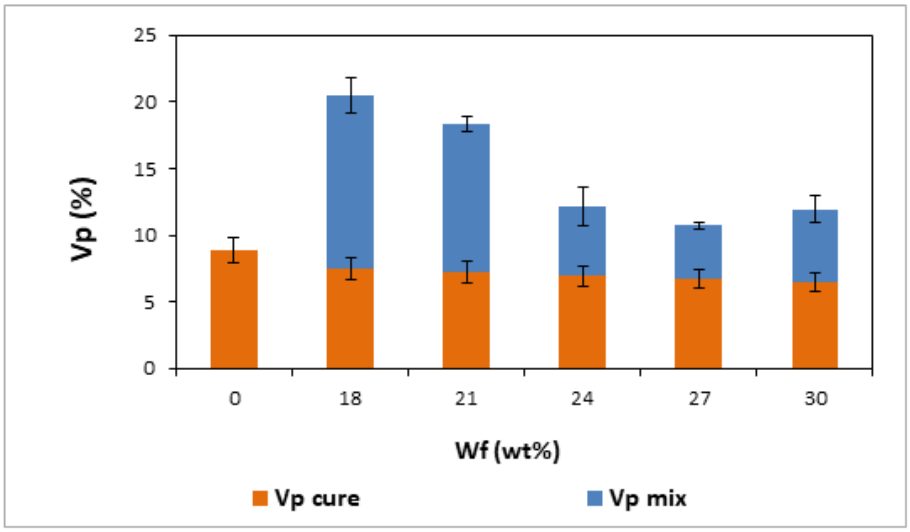


**Figure 11:** Porosity percentage in composites with different cellulose contents, cured at 90°C in the oven.

The porosity percentage doubled after the addition of 18 wt% of cellulose. Above 18 wt% of cellulose, the porosity decreased steadily when increasing the cellulose weight fraction. Owing to the particularly viscous and sticky nature of the PFA-Cell16-B slurry, the sudden increase in porosity when adding 18 wt% cellulose might be ascribed to air inclusion during the mixing and casting step and not only to water vapor generation during the thermal curing. In fact, this specific slurry was not as fluid as the pure PFA, which flowed easily in the molds. The stickiness of this particular slurry against the spatula further complicated the molding process leading to porosity embedding. For this reason, when the formulation started to be less sticky, casting was easier and voids inclusion was avoided. However, the porosity percentage of all the composites containing cellulose is higher than the neat PFA sample which is inconsistent with water content 30% lower than that of the bare resin. Therefore, the porosity volume ($V_p$) in the composites was mainly associated with the mixing and casting process ($V_{p\ mix}$). For a better understanding, the hypothesized internal composite structure is illustrated in Figure 9-(c) where red circles represent the porosity creating during the mixing and molding and those represented with blue circles present the porosity created later during curing. Accordingly, to estimate the porosity created during paste mixing and molding step ($V_{p\ mix)}$, few assumptions should be made, namely:

- The porosity volume created in the neat resin in the curing step ($V_{p\ cure}$) is not affected by the cellulose addition (neglecting the draining effect of fibers).

- Any porosity in the fibers is neglected.

In this case, the $V_{p\ cure}$ can be estimated based on the porosity of the neat PFA, which was found to be 8.9% using equation (3):

$$V_{p\ cure}\ (vol\%) = V_{p\ neat\ PFA}\ \cdot Vm \qquad (3)$$

Where $V_m$ is the volume fraction without considering any eventual porosity in the composite calculated using equation (4).

$$Vm\ (Vol\%) = \frac{V_{PFA}\ (cm^3) \cdot 100}{V_{PFA}\ (cm^3) + V_{cellulose}\ (cm^3)} \qquad (4)$$

Where $V_{PFA}\ (cm^3) = \frac{W_{PFA}\ (g)}{\rho_{PFA}}$ is the added oligomers volume inside the formulation, and $V_{Cellulose}\ (cm^3) = \frac{W_{cellulose}\ (g)}{\rho_{cellulose}}$ the added cellulose powder volume inside the formulation.

The porosity volume caused by the mixing can be therefore estimated as the difference between the total porosity and the porosity created in the resin phase during curing as:

$$V_{p\ mix}\ (vol\%) = V_p\ - V_{p\ cure} \qquad (5)$$

The effective volume fractions in the composite considering the pores volume can therefore be recalculated and the results are given in Table 4.

**Table 4:** Summary of the weight and volume fractions of different components and their respective shrinkage rates.

| | **Without porosity** | | | | **With porosity** | | | **Porosity origin** | | **Shrinkage** | |
|---|---|---|---|---|---|---|---|---|---|---|---|
| **Reference** | **Wm (wt%)** | **Wf (wt%)** | **Vf (vol%)** | **Vm (vol%)** | **Vm $_{eff}$ (vol%)** | **Vf $_{eff}$ (vol%)** | **Vp (vol%)** | **Vp $_{cure}$ (vol%)** | **Vp $_{mix}$ (vol%)** | **Shr. $_{exp}$** | **Shr. $_{theo}$** |
| **Neat PFA** | 100.0 | 0.0 | 0.0 | 100.0 | 91.2 | 0.0 | 8.8 | 8.8 | 0.0 | 2.9 | 2.9 |

| | Without porosity | | | | With porosity | | | Porosity origin | | Shrinkage | |
|---|---|---|---|---|---|---|---|---|---|---|---|
| **Reference** | **Wm (wt%)** | **Wf (wt%)** | **Vf (vol%)** | **Vm (vol%)** | **$Vm_{eff}$ (vol%)** | **$Vf_{eff}$ (vol%)** | **Vp (vol%)** | **$Vp_{cure}$ (vol%)** | **$Vp_{mix}$ (vol%)** | **$Shr._{exp}$** | **$Shr._{theo}$** |
| **PFA-Cell16-B** | 82.2 | 17.8 | 14.9 | 85.2 | 67.7 | 11.8 | 20.5 | 7.5 | 13.0 | 2.3 | 1.9 |
| **PFA- Cell19-B** | 78.7 | 21.3 | 17.9 | 82.1 | 67.0 | 14.6 | 18.4 | 7.2 | 11.2 | 1.3 | 1.9 |
| **PFA- Cell22-B** | 75.5 | 24.5 | 20.7 | 79.3 | 69.6 | 18.2 | 12.2 | 6.9 | 5.2 | 1.8 | 2.0 |
| **PFA- Cell25-B** | 72.6 | 27.5 | 23.4 | 76.6 | 68.4 | 20.9 | 10.8 | 6.7 | 4.0 | 1.9 | 1.9 |
| **PFA- Cell28-B** | 69.8 | 30.2 | 25.8 | 74.1 | 65.3 | 22.8 | 11.9 | 6.5 | 5.4 | 1.8 | 1.9 |

### 3.4.3 Shrinkage of the biocomposite

PFA, like the majority of thermosetting polymers, shrinks during curing, which, according to the supplier data, can reach 7%. The dimensional stability is important for composite production and 3D printing and it is, therefore, essential to minimize it. As shown in Figure 12, the shrinkage decreased when increasing the volume fraction of cellulose. Shrinkage upon curing of the PFA went from 2.9% for neat PFA to 1.8% when adding at least 24 wt% of cellulose fibers. The shrinkage of the resin is due to the evaporation of water and other volatiles during the curing process and the densification of the network. However, the cured composites have up to 35% of their volume occupied by dimensionally stable components (cellulose and pores), which could explain the shrinkage decrease. A theoretical shrinkage percentage was estimated by considering the shrinkage to be strictly related to the matrix phase shrinkage (which is estimated to be 2.9 %) using equation (6) and the resulting values are plotted in Figure 12.

$$\text{Shrinkage composite (\%)} = \frac{\text{Vm (vol\%)}}{100} \cdot \text{Shrinkage PFA (\%)} \qquad (6)$$

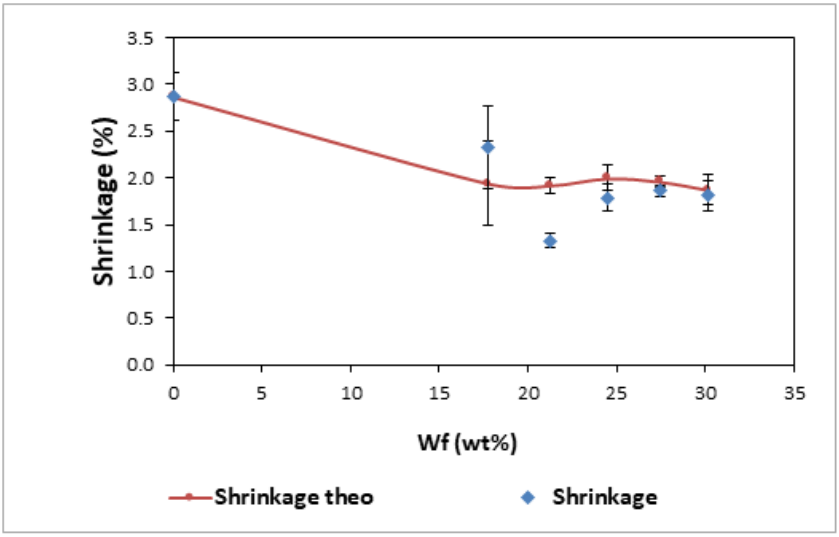


**Figure 12:** Shrinkage percentage of composites with different cellulose contents cured at 90°C in the oven.

Overall, cellulose addition has a major role in improving the composite dimensional stability during the curing process as shown by the fact that, under the tested conditions, cellulose decreased by 35% the shrinkage of the neat PFA down to 1.8% for the formulation PFA-Cell28-B (i.e. 3 times the usual shrinkage of ABS and PLA but less than the shrinkage of PP and PA which is over 2%). Cellulose addition can also prevent the foaming of the resin minimizing the curing porosity. It follows that, when avoiding air bubbles inclusion during the processing of the pasty formulation, the composite porosity can be decreased to less than 6%.

## 3.5 Thermal property

The thermal stability of the crosslinked PFA, cellulose and the composites was assessed by thermogravimetric analysis (TGA). The TGA curves given in Figure 13, show that in an oxidative atmosphere, cellulose loses 3% of its weight between 90 and 200°C, which is considered to be the residual moisture, followed by a classical abrupt degradation starting at 300°C, before a total degradation of the material when the temperature reaches 530°C. In the case of PFA, one notices a three-step degradation process. The first ramp starts at 200°C with only 10% weight loss, which could be explained by a further curing and consequent water evaporation [30]. The second step starts when the decomposition rate increases around 400°C to reach a 50% weight loss at 600°C, which is attributed to the

decomposition of the furan polymer [31]. The final degradation step leads to the total burning of the organic polymer at 700°C.

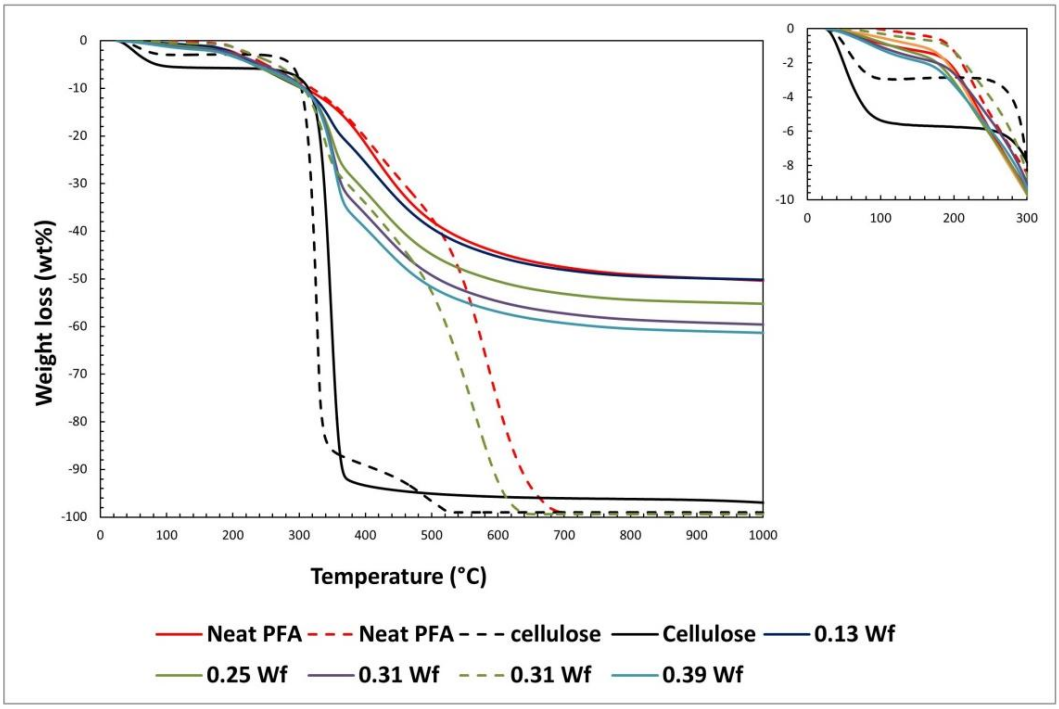


**Figure 13:** TGA scans collected at 10°C.min$^{-1}$ showing the degradation of cured neat PFA, cellulose powder, and biocomposites with different cellulose weight content under N2 (continuous curves) and under an oxygen atmosphere (dashed curves).

The degradation of the composites with 31 wt% cellulose content goes through the same 3 steps as for the neat PFA, with an increase in the cellulose decomposition temperature when the degradation rate increases, to reach a 25% weight loss at 400°C.

Under inert atmosphere ($N_2$), the degradation curves (Figure 13) show the same degradation steps, but the degradation rate decreases considerably starting from 500°C to reach a plateau at 800°C. After the stabilization of the weight loss, the char residue is about 50 wt%, which is in agreement with values given in the literature [1]. This residue decreases when increasing the thermally unstable cellulose fraction that loses up to 90% of its initial weight. The char residue of the composite with more than 30 wt% of cellulose is around 40 wt%, which therefore does not exclude the possibility of carbonization of the molded composites.

## 3.6 Thermomechanical behavior

The storage modulus E' of composites as a function of temperature is given in Figure 14. Cellulose addition increased the storage modulus of the composites, which is higher than that of the neat cured PFA over the whole temperature region. This could be ascribed to the tension transfer from the matrix to the high-modulus filler, which enhanced the composite stiffness.

At room temperature, the modulus E' increased when increasing the cellulose fraction, which was maximized for $W_f$= 30 wt%. Cellulose addition also improved the composite thermomechanical stability by increasing the stiffness at high temperatures. For instance, with a 30 wt% weight fraction of cellulose, the modulus remained higher than 4 GPa up to 150°C and higher than 2 GPa up to 200°C, whereas, for the neat cured PFA, it dropped below 2 GPa when reaching 150°C. The thermal stability and the rigidity of both the cured neat PFA and the composites were higher than those reported in the literature when incorporating sisal whiskers and lignin in conventional PFA [2, 11]. In addition to the typical thermomechanical stability of cellulose fibers, cellulose microparticles are supposed to hinder polymer chains mobility thus further enhancing the composite thermomechanical behavior.

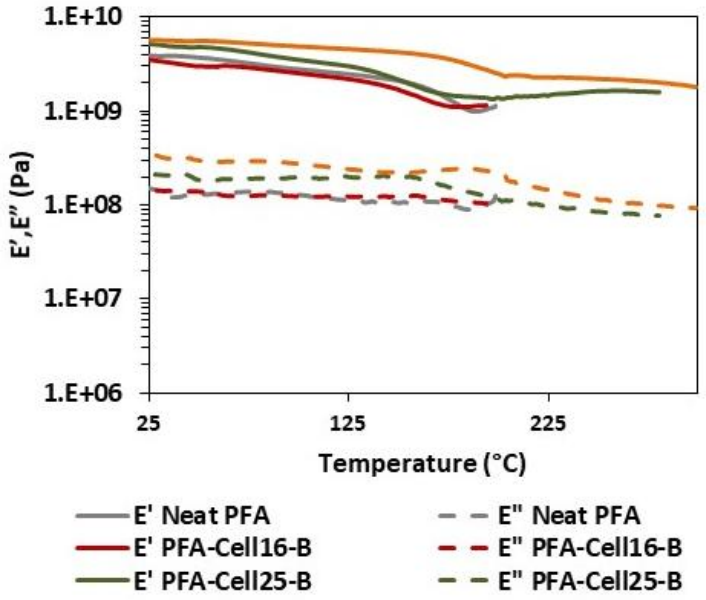


**Figure 14:** Storage (continuous curves) and loss (dashed curves) moduli of composites with different cellulose weight fraction plotted as a function of temperature.

This thermomechanical stability is competitive with those of PEEK and some other technical polymers used in 3D printing [32–36]. Unlike the PFA/cellulose composite, these technical thermoplastics can be extremely expensive and also rather complicated to print, apart from the fact that they are fossil-based materials.

## 3.7 Mechanical performances

As can be seen in Figure 15, the composite stiffness improved after the addition of cellulose powder. The tensile modulus increased from 2527 to 2880 MPa and the flexural modulus from 3092 to 4309 MPa by adding 30 wt% of cellulose. This modest improvement suggests a good wetting by the resin of the cellulose particles [37] and agrees well with the DMA results.

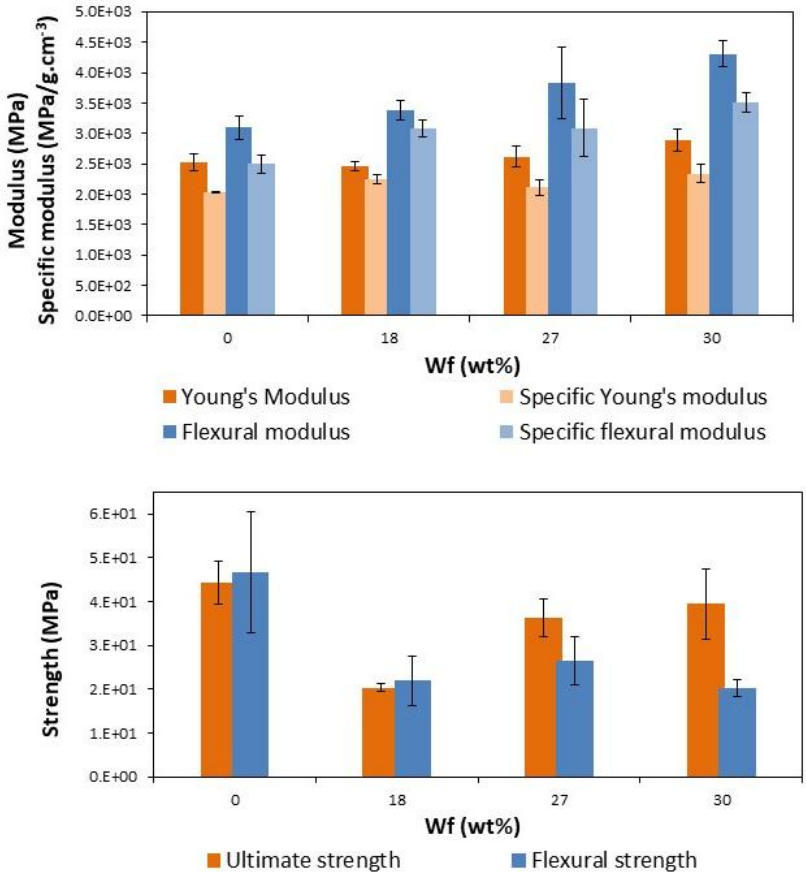


**Figure 15:** Tensile and flexural modulus and strengths of neat cured PFA and different biocomposites.

On the other hand, the tensile and flexural strength decreased when adding cellulose with an opposite evolution of porosity. This can be explained by the fact that high porosity content in the composite is deteriorating the strength

because pores act as stress concentrators and fracture nucleation sites [38]. Therefore, when recalculating the specific modulus by normalizing the measured values to their density, one can notice that cellulose is improving the mechanical properties of the composite by increasing the flexural modulus by 40% and tensile modulus by 10%. Therefore, voids generated during the paste preparation and manual casting are supposed to be at the origin of the limited enhancement of the mechanical performance of the tested samples.

## 3.8 Biocomposite's applications

Owing to its interesting thermal and mechanical properties, the developed new biocomposite might be used in technical applications such as in automobile, transport fields and for industrial uses in general. However, due to the particular nature of the pasty composite precursor, an adapted manufacturing process should be found. To this end, the use of the novel manufacturing process of additive manufacturing is possible thanks to the rheological properties of the developed slurry. Indeed, these rheological properties, open the possibility of using a special 3D printing technique called DIW (direct ink writing) where a pasty material is pushed through a nozzle and deposited layer per layer without heating followed by a solidification step by crosslinking the thermosetting polymer. As one can see, in Figure 16-(a) a gear made of the formulation PFA-Cell28-B was successfully printed and solidified. This case of application was described and studied in detail in a previous study [39]. The pasty precursor can also be molded using compression molding to produce mainly thin pieces to avoid the phenomenon of porosity formation mentioned earlier. The paste is placed in a heated mold and spread into the mold's form thanks to an applied pressure (between 2 and 4 MPa). The mold is then mantained heated to crosslink and solidify the composite to obtain, as we can see in Figure 16-(b) a solid biocomposite which is in this case a 4mm-thick sheet. This sheet can be machined (milling, drilling, shaping, CNC) to manufacture a more specific shape. To implement the use of these manufacturing processes, a demonstrator of a gear pump was manufactured using machined molded biocomposite plates, to shape the casing in which two 3D-printed gears are housed as demonstrated in Figure 16-(c).

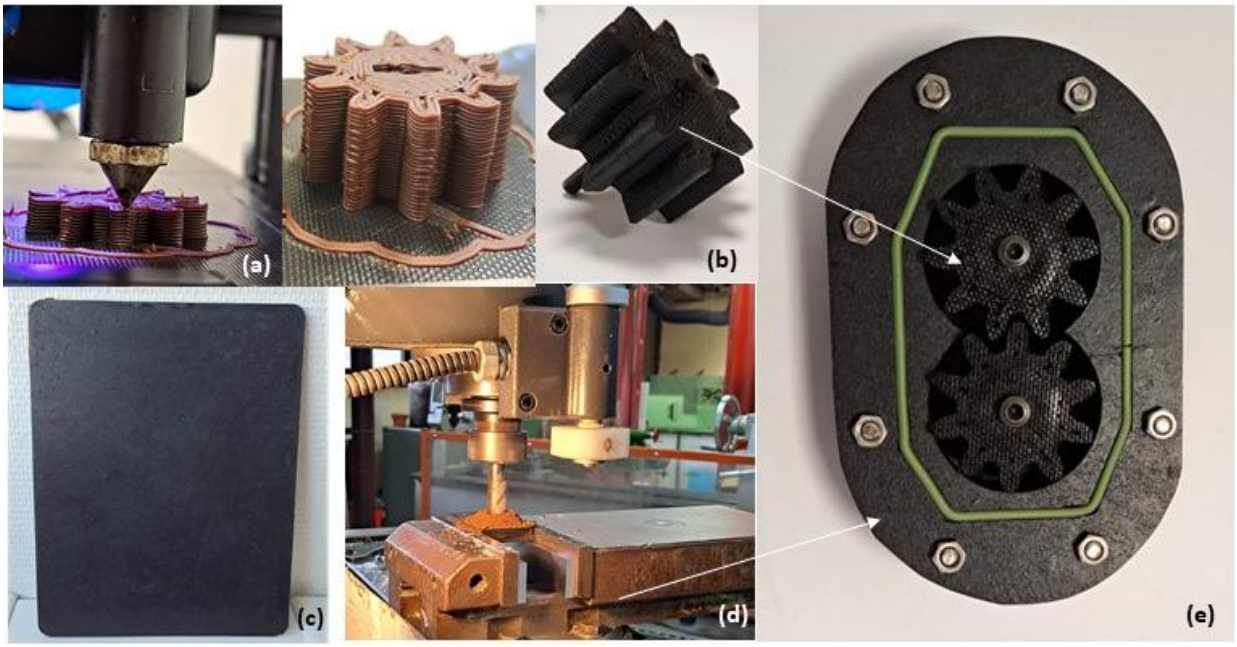


**Figure 16:** Application cases of the developed biocomposite using (a) DIW 3D printing process to manufacture (b) a gear and (c) compression molding to obtain a 4 mm thick composite sheet. The composite sheet was further (d) machined to shape a gear pump casing. (e) The two 3D-printed gears were fixed in the machined pump casing to obtain a static gear pump demonstrator.

## 4 CONCLUSION

In the present study, the production of fully bio-based composites by the air casting of a commercial oligomeric furan resin with a curing catalyst and cellulose powder slurries was readily achieved. The experimental results demonstrated that:

- The cellulose addition induced porosity during manual paste lay-out caused by its high viscosity and sticky nature. After adding 18 wt% cellulose the porosity increased by 125% with respect to the pure matrix, but gradually decreased when adding more cellulose until reaching a plateau value of 11%. Despite the increase in the overall porosity, the cellulose fibers limited the resin foaming during the thermal curing at high temperature. This phenomenon was associated to composite degassing by vapor diffusion through the cellulose percolation network. The porosity content of these composites could be further minimized by applying a pressure to the curing process instead of the simple air curing process chosen in this study.

- The dimensional stability of the resulting composites increased by 35% when adding 30 wt% of cellulose with respect to the cured matrix.
- The thermo-mechanical stability was improved by adding the cellulose fillers. The storage modulus improved by 60% at room temperature and by 125% at 150 °C when adding 30 wt% of cellulose. Moreover, composites were thermally stable up to 200°C, unlike the cured neat matrix. In addition, according to the TGA curves, the composites, like the matrix, showed excellent thermal stability with 40-50% char residue. Nevertheless, the mass loss due to the cellulose degradation (300 °C) was more important for the composites compared to that of the matrix.
- Despite the high cellulose content, the composites were insensitive to humidity with less than 0.05% weight gain when placed in 90% RH for two hours.
- Finally, mechanical performances were enhanced when adding the cellulose filler. The specific tensile and flexural modulus were improved from 2.04 to 2.34 GPa/g.cm$^{-3}$ and from 2.49 to 3.5 GPa/g.cm$^{-3}$, respectively.

## AUTHOR INFORMATION


### Corresponding Author

* K. Bouzidi Univ. Grenoble Alpes, CNRS, Grenoble INP, LGP2

E-mail: Khaoula.Bouzidi@grenoble-inp.fr


### Author Contributions

The manuscript was written through contributions of all authors. All authors have given approval to the final version of the manuscript. All authors contributed equally.

## ACKNOWLEDGEMENT


The authors would like to acknowledge Transfurans Chemicals for generously providing the furan resin and the curing agent used in this work.


## COMPLIANCE WITH ETHICAL STANDARDS


**Funding:** This study was funded by the Region Auvergne Rhone Alpes (Grant: 3D-PapEl, 1701107001-22437-) and the LabCom IDEX Université Grenoble Alpes (Grant: 2018/2019 ThermoBioComp3D).

**Conflict of Interest:** The authors declare that they have no conflict of interest.

## REFERENCES


1. Gandini A (1997) Furans in polymer chemistry. Progress in Polymer Science 22:1203–1379. https://doi.org/10.1016/S0079-6700(97)00004-X

2. Guigo N, Mija A, Vincent L, Sbirrazzuoli N (2010) Eco-friendly composite resins based on renewable biomass resources: Polyfurfuryl alcohol/lignin thermosets. European Polymer Journal 46:1016–1023. https://doi.org/10.1016/j.eurpolymj.2010.02.010

3. Choura M, Belgacem NM, Gandini A (1996) Acid-Catalyzed Polycondensation of Furfuryl Alcohol: Mechanisms of Chromophore Formation and Cross-Linking. Macromolecules 29:3839–3850. https://doi.org/10.1021/ma951522f

4. Tondi G, Cefarin N, Sepperer T, et al (2019) Understanding the Polymerization of Polyfurfuryl Alcohol: Ring Opening and Diels-Alder Reactions. Polymers 2019:2126. https://doi.org/10.3390/polym11122126

5. Deka H, Misra M, Mohanty A (2013) Renewable resource based "all green composites" from kenaf biofiber and poly(furfuryl alcohol) bioresin. Industrial Crops and Products 41:94–101. https://doi.org/10.1016/j.indcrop.2012.03.037

6. Pohl T, Bierer M, Natter E, et al (2011) Properties of compression moulded new fully biobased thermoset composites with aligned flax fibre textiles. Plastics, Rubber and Composites 40:294–299. https://doi.org/10.1179/1743289810Y.0000000017

7. Domínguez JC, Grivel JC, Madsen B (2012) Study on the non-isothermal curing kinetics of a polyfurfuryl alcohol bioresin by DSC using different amounts of catalyst. Thermochimica Acta 529:29–35. https://doi.org/10.1016/j.tca.2011.11.018

8. Oishi SS, Rezende MC, Origo FD, et al (2013) Viscosity, pH, and moisture effect in the porosity of poly(furfuryl alcohol). Journal of Applied Polymer Science 128:1680–1686. https://doi.org/10.1002/app.38332

9. Pin J-M, Guigo N, Mija A, et al (2014) Valorization of Biorefinery Side-Stream Products: Combination of Humins with Polyfurfuryl Alcohol for Composite Elaboration. ACS Sustainable Chemistry & Engineering 2:2182–2190. https://doi.org/10.1021/sc5003769

10. Menager C, Guigo N, Wu X, et al (2019) "Green" composites prepared from polyfurfuryl alcohol and cork residues: Thermal and mechanical properties. Composites Part A: Applied Science and Manufacturing 124:105473. https://doi.org/10.1016/j.compositesa.2019.105473

11. Ahmad EEM, Luyt AS, Djoković V (2013) Thermal and dynamic mechanical properties of bio-based poly(furfuryl alcohol)/sisal whiskers nanocomposites. Polymer Bulletin 70:1265–1276. https://doi.org/10.1007/s00289-012-0847-2

12. Lems E-M, Winklehner S, Hansmann C, et al (2019) Reinforcing effect of poly(furfuryl alcohol) in cellulose-based porous materials. Cellulose 26:4431–4444. https://doi.org/10.1007/s10570-019-02348-6

13. Wang Y, Deng L, Xiao Z, et al (2019) Preparation and properties of bamboo/polymer composites enhanced by in situ polymerization of furfuryl alcohol. Materials Express 9:712–722. https://doi.org/10.1166/mex.2019.1550

14. Kherroub D, Belbachir M, Lamouri S (2015) Synthesis of poly(furfuryl alcohol)/montmorillonite nanocomposites by direct in-situ polymerization. Bulletin of Materials Science 38:. https://doi.org/10.1007/s12034-014-0818-3

15. Toriz G, Arvidsson R, Westin M, Gatenholm P (2003) Novel cellulose ester–poly(furfuryl alcohol)–flax fiber biocomposites. Journal of Applied Polymer Science 88:337–345. https://doi.org/10.1002/app.11730

16. Giannis S, Arnold E, Hoydonckx HE, et al (2008) Development of high performance bio-composites based on furan bio-resins for vehicle panels. 13th European Conference on Composite Materials 10

17. Pranger LA, Nunnery GA, Tannenbaum R (2012) Mechanism of the nanoparticle-catalyzed polymerization of furfuryl alcohol and the thermal and mechanical properties of the resulting nanocomposites. Composites Part B: Engineering 43:1139–1146. https://doi.org/10.1016/j.compositesb.2011.08.010

18. Crossley RJ, Schubel PJ, Stevenson A, Moreira M (2012) The development and processing of a sustainable fully bio derived polyfurfuryl alcohol matrix flax fibre prepreg. 8

19. Malaba T, Wang J (2015) Unidirectional Cordenka Fibre-Reinforced Furan Resin Full Biocomposite: Properties and Influence of High Fibre Mass Fraction. Journal of Composites 2015:e707151. https://doi.org/10.1155/2015/707151

20. Behzadfar A, Imani M, Farahmandghavi F (2019) Shelf-life of polyfurfuryl alcohol resin: an accelerated rheokinetics study. Polym Bull 76:5903–5918. https://doi.org/10.1007/s00289-019-02692-4

21. González R, Figueroa JM, González H (2002) Furfuryl alcohol polymerisation by iodine in methylene chloride. European Polymer Journal 38:287–297. https://doi.org/10.1016/S0014-3057(01)00090-8

22. Principe M, Ortiz P, Martínez R (1999) An NMR study of poly(furfuryl alcohol) prepared with p-toluenesulphonic acid. Polymer International 48:637–641. https://doi.org/10.1002/(SICI)1097-0126(199908)48:8<637::AID-PI206>3.0.CO;2-C

23. Chuang IS, Maciel GE, Myers GE (1984) Carbon-13 NMR study of curing in furfuryl alcohol resins. Macromolecules 17:1087–1090. https://doi.org/10.1021/ma00135a019

24. Montserrat S, Flaqué C, Calafell M, et al (1995) Influence of the accelerator concentration on the curing reaction of an epoxy-anhydride system. Thermochimica Acta 269–270:213–229. https://doi.org/10.1016/0040-6031(95)02362-3

25. Ooi SK, Cook WD, Simon GP, Such CH (2000) DSC studies of the curing mechanisms and kinetics of DGEBA using imidazole curing agents. Polymer 41:3639–3649. https://doi.org/10.1016/S0032-3861(99)00600-X

26. Mokhothu TH, John MJ (2017) Bio-based coatings for reducing water sorption in natural fibre reinforced composites. Sci Rep 7:13335. https://doi.org/10.1038/s41598-017-13859-2

27. Dong Y, Yan Y, Zhang S, Li J (2014) Wood/Polymer Nanocomposites Prepared by Impregnation with Furfuryl Alcohol and Nano-SiO2. BioResources 9:6028–6040

28. Kumar R, Kumar R, Anandjiwala R (2012) Biofilms from soy protein isolate and polyfurfuryl alcohol. Plastics, Rubber and Composites 41:1–7. https://doi.org/10.1179/1743289811Y.0000000002

29. Domínguez J, Madsen B (2015) Development of new biomass-based furan/glass composites manufactured by the double-vacuum-bag technique. Journal of Composite Materials 49:2993–3003. https://doi.org/10.1177/0021998314559060

30. Ma CCM, Yn MS, Han JL, et al (1995) Pultruded fibre-reinforced furfuryl alcohol resin composites: 1. Process feasibility study. Composites Manufacturing 6:45–52. https://doi.org/10.1016/0956-7143(95)93712-S

31. Guigo N, Mija A, Zavaglia R, et al (2009) New insights on the thermal degradation pathways of neat poly(furfuryl alcohol) and poly(furfuryl alcohol)/SiO2 hybrid materials. Polymer Degradation and Stability 94:908–913. https://doi.org/10.1016/j.polymdegradstab.2009.03.008

32. Diez-Pascual A, Naffakh M, Gómez M, et al (2009) The influence of a compatibilizer on the thermal and dynamic mechanical properties of PEEK/carbon nanotube composites. Nanotechnology 20:315707. https://doi.org/10.1088/0957-4484/20/31/315707

33. Cao Z, Qiu L, Yang Y, et al (2015) The surface modifications of multi-walled carbon nanotubes for multi-walled carbon nanotube/poly(ether ether ketone) composites. Applied Surface Science 353:873–881. https://doi.org/10.1016/j.apsusc.2015.07.025

34. Qu S, Penaranda J, Wang S-S (2017) Elevated-Temperature Wear and Friction of PTFE/PEEK composite

35. Papageorgiou DG, Liu M, Li Z, et al (2019) Hybrid poly(ether ether ketone) composites reinforced with a combination of carbon fibres and graphene nanoplatelets. Composites Science and Technology 175:60–68. https://doi.org/10.1016/j.compscitech.2019.03.006

36. Niu Y, Zheng S, Song P, et al (2021) Mechanical and thermal properties of PEEK composites by incorporating inorganic particles modified phosphates. Composites Part B: Engineering 212:108715. https://doi.org/10.1016/j.compositesb.2021.108715

37. Ku H, Wang H, Pattarachaiyakoop N, Trada M (2011) A review on the tensile properties of natural fiber reinforced polymer composites. Composites Part B: Engineering 42:856–873. https://doi.org/10.1016/j.compositesb.2011.01.010

38. Pfister DP, Larock RC (2010) Green composites from a conjugated linseed oil-based resin and wheat straw. Composites Part A: Applied Science and Manufacturing 41:1279–1288. https://doi.org/10.1016/j.compositesa.2010.05.012

39. Bouzidi K, Chaussy D, Gandini A, et al (2022) 3D printable fully biomass-based composite using poly(furfuryl alcohol) as binder and cellulose as a filler. Carbohydrate Polymers 293:119716. https://doi.org/10.1016/j.carbpol.2022.119716